JACS
JOURNAL OF THE AMERICAN CHEMICAL SOCIETY

Article

pubs.acs.org/JACS

Atomistic Study of Energy Funneling in the Light-Harvesting Complex of Green Sulfur Bacteria

Joonsuk Huh,*[,†] Semion K. Saikin,[†] Jennifer C. Brookes,[†,‡] Stéphanie Valleau,[†] Takatoshi Fujita,[†] and Alán Aspuru-Guzik*[,†]

[†]Department of Chemistry and Chemical Biology, Harvard University, Cambridge, Massachusetts 02138, United States
[‡]Department of Physics and Astronomy, University College London, Gower, London WC1E 6BT, United Kingdom

Supporting Information

ABSTRACT: Phototrophic organisms such as plants, photosynthetic bacteria, and algae use microscopic complexes of pigment molecules to absorb sunlight. Within the light-harvesting complexes, which frequently have several functional and structural subunits, the energy is transferred in the form of molecular excitations with very high efficiency. Green sulfur bacteria are considered to be among the most efficient light-harvesting organisms. Despite multiple experimental and theoretical studies of these bacteria, the physical origin of the efficient and robust energy transfer in their light-harvesting complexes is not well understood. To study excitation dynamics at the systems level, we introduce an atomistic model that mimics a complete light-harvesting apparatus of green sulfur bacteria. The model contains approximately 4000 pigment molecules and comprises a double wall roll for the chlorosome, a baseplate, and six Fenna-Matthews-Olson trimer complexes. We show that the fast relaxation within functional subunits combined with the transfer between collective excited states of pigments can result in robust energy funneling to the initial excitation conditions and temperature changes. Moreover, the same mechanism describes the coexistence of multiple time scales of excitation dynamics frequently observed in ultrafast optical experiments. While our findings support the hypothesis of supertransfer, the model reveals energy transport through multiple channels on different length scales.

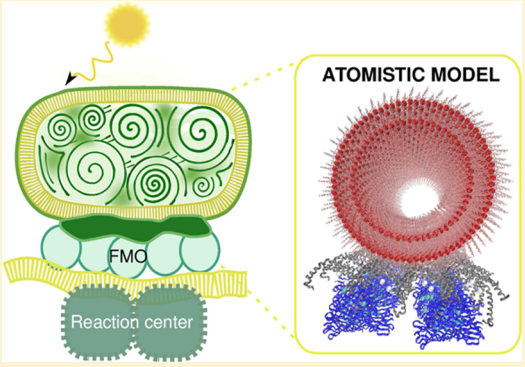

INTRODUCTION

Photosynthetic bacteria are among the simplest organisms on Earth, which use sunlight as their main energy source.[1] To collect solar energy, these bacteria exploit light-harvesting complexes (LHC), aggregates of pigment molecules, which absorb photons and transfer the associated energy at the submicrometer scale. The LHC in green sulfur bacteria contains large light absorbing antennae self-assembled in the so-called chlorosome.[2] These bacteria are obligate phototrophs; they are required to use sunlight to support metabolic reactions.[3−5] However, it has been observed that green sulfur bacteria can live in extremely low light conditions, even when receiving only a few hundred photons per bacterium per second.[6−8] These facts have inspired many conjectures and discussions on the functional properties, energy conversion efficiency, and robustness of LHC in green sulfur bacteria.[9−15]

To address this controversy, we introduce a model that includes atomistic structural detail of the green bacteria LHC and allows for the simulation of excitation energy transfer (EET) at the systems level. As a specific example, we consider the LHC of *Chlorobium tepidum*. We observe fast relaxation of excitations within the subunits of LHC due to the large overlap between exciton states and strong interaction with environmental fluctuations. The transfer between subunits involves collective excited states of the pigment molecules and supports the hypothesis of supertransfer.[12,14,15] The energy transport is robust to different initial excitation conditions and changes in temperature. Finally, we show that the population of different parts of the LHC can be described using simple kinetic equations with time-dependent transfer rates characterizing intraunit dynamics. This later model naturally explains the multiple time scales of EET reported in optical studies of green sulfur bacteria[16−20] and green nonsulfur bacteria.[21−23]

Theoretical models have been applied mostly to single functional units of LHCs[24−35] to understand the physical principles of energy transfer. Some of these studies also involved atomistic structures,[30,32,36,37] which make the models computationally demanding. To the authors' knowledge, there are only a few atomistic studies of the complete light-harvesting systems of purple bacteria,[38,39] but none for green sulfur bacteria. In addition to the large-scale calculations, the detailed analysis of excitation dynamics on the systems level[23,38−41] is complicated due to the lack of structural information. Thus, one usually needs to use macroscopic phenomenological models[42] or introduce additional constraints and approximations on the transport models.[43−45]

Received: November 25, 2013
Published: January 9, 2014

   dx.doi.org/10.1021/ja412035q | *J. Am. Chem. Soc.* 2014, 136, 2048−2057

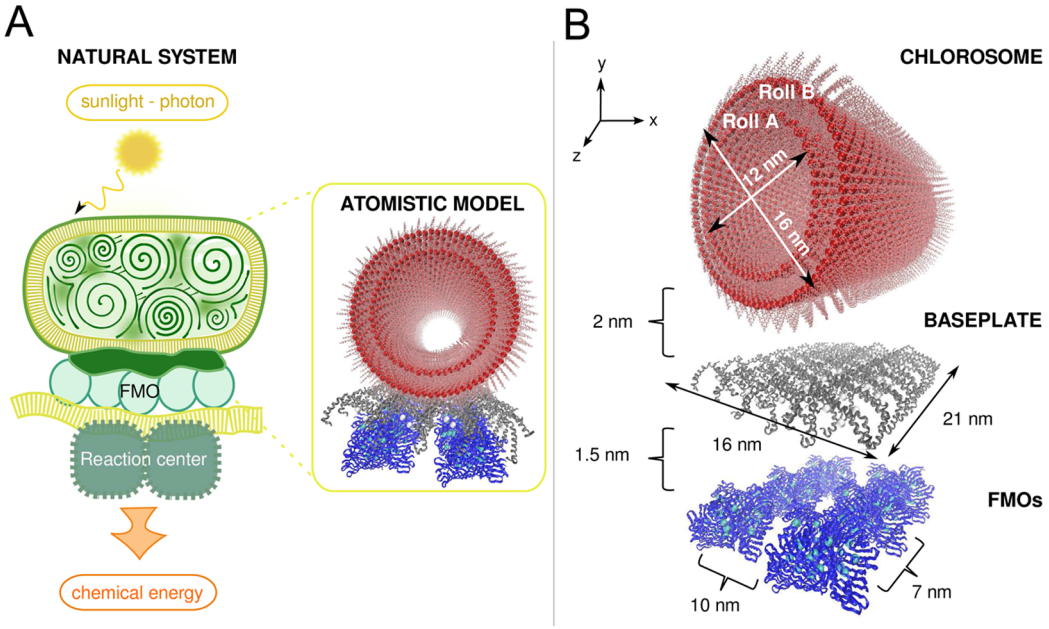

Figure 1. Photosynthetic apparatus. (A) Cartoon of light-harvesting complex in green sulfur bacteria. The bacteria transform solar photons into chemical energy. Sunlight absorbed by the chlorosome is transferred in the form of an exciton through the baseplate and Fenna-Matthews-Olson (FMO) complexes subsequently to the reaction center. A snapshot of the model structure is also shown. (B) Atomistic model with corresponding length scales. The atomistic model is composed of a double wall roll for the chlorosome (roll A, 1620 (= 60 × 27) BChl *c* sites; and roll B, 2160 (= 80 × 27) BChl *c* sites), baseplate (64 BChl *a* sites), and 6 FMO trimer complexes (144 (= 24 × 6) BChl *a* sites).

The LHC in green sulfur bacteria is composed of bacteriochlorophyll (BChl) pigment molecules. These monomers aggregate in several interconnected functional units, as shown in Figure 1A. The main element of LHC is the chlorosome, an ellipsoidal shaped body of size ranging from tens to hundreds of nanometers.[2] The chlorosome is densely packed with BChl *c* pigments. Two other functional units, the baseplate[46] and the Fenna-Matthews-Olson (FMO) trimer complex,[47] are composed of BChl *a* pigments held together by a protein scaffolding. Energy in the form of molecular excitations (i.e., exciton) is collected by the chlorosome and funneled through these antenna units to the reaction center where charge carriers are then generated. The distance between the pigments in LHCs is sufficiently large such that the overlap of electronic wave functions can be neglected. In this case, the energy transfer is mediated by the near field interaction between molecular electronic transitions, the Förster interaction.[48−50] If the interaction between several molecules is sufficiently strong as compared to the energy difference between their electronic transitions, the exciton states are delocalized over the group of pigments.[49,50] The preferential direction for energy transport is controlled by the frequencies of electronic transitions: the excitation goes to molecules or groups of molecules with lower excited state energy, while dissipating the energy difference to the environment.

MOLECULAR AGGREGATE MODEL

A single LHC of *Chlorobium tepidum* contains 200−250 thousand BChl molecules.[2,19,51] Most of these molecules are found in the chlorosome. The model we have created is shown in Figure 1; it is composed of 3988 pigments and represents all of the functional units of LHC in green sulfur bacteria, excluding the reaction center.

In our model (Figure 1B), a double wall roll aggregate with diameter of about 16 nm and length of about 21 nm represents the chlorosome. Several possible structural arrangements of BChls in the chlorosome have been investigated theoretically and experimentally.[52−58] Here, we use the structure of Ganapathy et al.,[56] obtained from a triple mutant bacteria and characterized with nuclear magnetic resonance and cryo-electron microscopy. This structure is also supported by two-dimensional polarization fluorescence microscopy experiments.[59]

The microscopic structure of the baseplate has not yet been experimentally verified.[46] We construct a baseplate lattice as follows. The unit cell consists of dimers of CsmA proteins[60] containing 2 BChl *a* molecules sandwiched between the hydrophobic regions and bound near the histidine. To establish a stable structure of the baseplate, classical molecular dynamics simulations were done. (The NAMD program package version 2.8[61] was used. Force fields were parametrized with a combination of Amber ff99SB for the protein[62] and MMFF94 atomic charges for the BChl *a*.) The final structure complies with the periodicity and dimensions of the unit cell as seen in freeze frame fracture.[63] The lattice model for the baseplate is described in the Supporting Information. Finally, for the FMO protein complexes, we employ the structure resolved by Tronrud et al.[64]

The ratio of BChl *c* in the chlorosome to BChl *a* in the baseplate (98.3:1.7) is comparable to the stochiometry of the natural system (99:1, approximately).[2,19] The estimated density of FMO complexes is about 1 FMO/50 nm^2.[65] Therefore, we distribute 6 FMO complexes under the baseplate, which occupies about 300 nm^2 (see Figure 1B). This gives a pigment ratio of 2.3:1 (FMOs:baseplate), which is similar to the corresponding stochiometry of *Chlorobium tepidum* 2:1.[51]

The distances between the chlorosome BChl *c* aggregates and the baseplate are determined by the length of BChl *c* esterifying alcohols. In the case of *Chlorobium tepidum*, it is about 2 nm.[20,23,46] While the orientation of FMO relative to the

dx.doi.org/10.1021/ja412035q | J. Am. Chem. Soc. 2014, 136, 2048−2057

baseplate has been verified experimentally,[65] the relative distance between these units is unknown. In our model we set it to be 1.5 nm, which is larger than the interpigment distance within FMO but smaller than the baseplate-chlorosome distance. This choice is based on the argument that the FMO complex is strongly linked to the baseplate.[66] Minor variations of this distance do not affect the results.

The frequencies of exciton transitions in LHCs are controlled by multiple factors. In the model it is equivalent to use the relative shifts (energy gap) of these transitions, which are relevant to the EET. These shifts can be calculated from the pigment-pigment couplings and the electronic excitations of single BChls, site energies, modified by the local environment.[67] While the couplings can straightforwardly be computed using a screened dipole-dipole model,[67] the calculation of site energies requires more complicated models or fitting to experimentally measured optical spectra. Here, we set the frequency offset to be aligned with the lowest site energy of the FMO complex.[66,68]

The absorption domains of the baseplate and FMO composed of BChl *a* pigments are not clearly distinguishable. The absorption band of the baseplate covers the range 790–810 nm. This range also includes the absorption band of the FMO complexes.[20,68,69] In fact, the absorption band of the baseplate significantly overlaps with that of the chlorosome.[20] To reproduce these spectra using the constructed model, we define the site energy of BChl *c* to be 2950 cm^{-1}, which places the absorption maximum of the chlorosome of about 640 cm^{-1} above the absorption maximum of FMO complexes (see Figure 2A). Our choice is based on the fluorescence maximum of the chlorosome (786 nm).[20] We shift the lowest exciton state obtained after taking 1000 ensemble average over the site energy fluctuation (standard deviation: 500 cm^{-1} [70]) at the fluorescence maximum. 12 225 cm^{-1} (818 nm) is used as the offset energy value. We assign the site energy of the baseplate as 550 cm^{-1}, which places the absorption maximum of the baseplate approximately in the middle of the absorption maxima of the FMO complexes and the chlorosome. The resulting absorption spectrum of the baseplate is shown in Figure 2A.

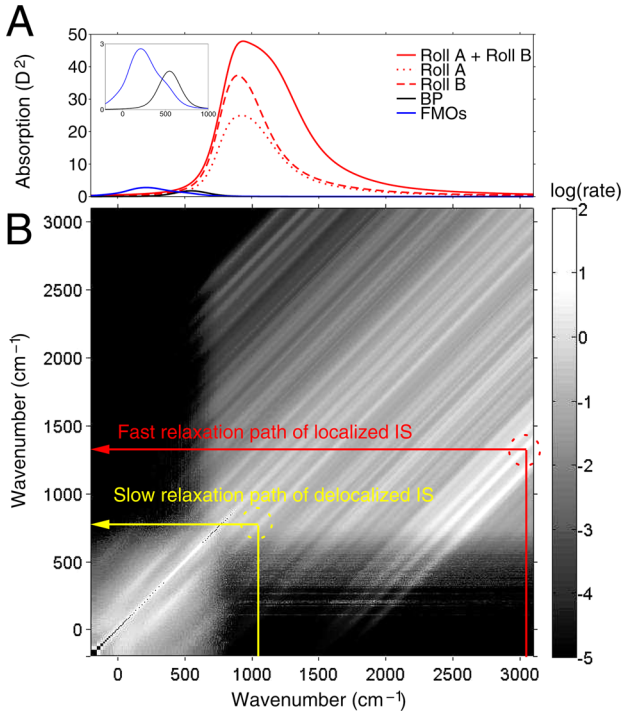

Figure 2. Calculated absorption spectra and exciton transfer rate matrix γ_{MN}. (A) Calculated absorption spectra[92] by direct diagonalization of the system Hamiltonians of the antenna units are shown. The absorption spectra are calculated and drawn for the double wall roll (roll A + roll B), the single rolls (roll A and roll B), the baseplate, and the 6 FMO complexes. The absorption spectrum of each antenna unit is obtained after taking 1000 ensemble average over the site energy fluctuations (static disorder). A Lorentzian line shape function with a full width at half-maximum of 100 cm^{-1} is convoluted, additionally, to take the homogeneous broadening into account. The inset is shown to magnify the spectra of the baseplate and FMO complexes in the original plot. (B) Transfer rate matrix γ_{MN} (cm^{-1}) at 300 K is presented in a logarithmic scale. γ_{MN} indicates population transfer rate between exciton states $|M\rangle$ and $|N\rangle$. We set here the frequency offset to be aligned with the lowest site energy of the FMO complex.

EXCITON TRANSFER MODEL

The exciton transfer is modeled with a quantum master equation approach, which includes the coherent, dephasing, and relaxation processes, for the open quantum dynamics.[67,71−74] We solve the quantum master equation to obtain the spacial distribution of the exciton.

In our model, the system-bath Hamiltonian of the light-harvesting apparatus is composed of three parts: the system consists of the local excitations of bacteriochlorophylls (BChls) and the point dipole interactions between them, described using a tight-binding Hamiltonian. The system (BChls) then is coupled linearly to the bath (proteins). The bath Hamiltonian consists of a sum of multidimensional quantum harmonic oscillators (see, e.g., ref 74 and the Supporting Information). (In general, the extended dipole or the transition charges from the electrostatic potentials (TrEsp) models for BChls may give more precise values for the electronic couplings. In Fujita et al.,[75] we did a careful study of the TrEsp couplings and found that the TrEsp model can produce a 2−3 times longer decoherence times as compared to the point dipole model. However, the point dipole model can reproduce the proper experimental red shift for the chlorosome. Moreover, in the energy funneling process, we expect the relative energy gaps are more important than the internal dynamics within an antenna unit because the time scale of the internal dynamics is faster than the energy transfer between different energy transfer units. In the TrEsp model,[75] the electronic coupling strength between the pigments more than 2 nm apart is similar to the point dipole approximation. Therefore, we expect that the use of the more sophisticated model has a minor effect on the time scales between the antenna units, which is the main focus of this Article.)

Within the secular approximation and in the Markov limit (i.e., secular Redfield), the equations of motion of the reduced density operator $\hat{\rho}_S(t)$ in the exciton basis, the population and coherence transfer are decoupled.[76] The equations of motion are given in the Supporting Information.

The resulting quantum master equation includes a term γ_{MN}, which is the exciton transition rate between the corresponding exciton states $|M\rangle$ and $|N\rangle$. γ_{MN} is calculated with the exciton eigenvectors and spectral density (exciton-phonon coupling strength) at the transition energy (see refs 74,77 for the definition and also the Supporting Information for the expressions). It is shown in Figure 2B as a matrix, for the EET dynamics at 300 K.

dx.doi.org/10.1021/ja412035q | J. Am. Chem. Soc. 2014, 136, 2048−2057

The validity of the Redfield method for the EET in natural light-harvesting structures had been discussed by many authors, see, for example, refs 76,78−82 and the references cited therein. When the energy gap between the exciton states is small, the Redfield model with a broad spectral density can be applicable.[80] Our molecular aggregate model in Figure 1 and the corresponding spectral densities[30,70] satisfy this condition: the absorption spectra of the antenna units overlap each other significantly, which implies the exciton states in this energy domain are delocalized over the two antenna units. The antenna units are coupled weakly (16−17 cm^{-1}). The spectral densities and the density of states are given in the Supporting Information.

Novoderezhkin and et al.[81] proposed to compensate the underestimation of the transfer rate between exciton states with large energy gaps by increasing the spectral density in the high frequency region. Therefore, we note here the exciton transition rate, which involves the exciton transfer with a large energy gap, could be underestimated because the Redfield model can only account for the single phonon process. Multiphonon processes could occur in the internal exciton dynamics of the antenna units due to its broad exciton bands (see Figure 2A). The internal exciton dynamics of the chlorosome is, however, much faster than the exciton transfer between the antenna units. Thus, the Redfield model should give a reasonable result (time scales) qualitatively for the exciton funneling process of the photosynthetic apparatus. For more accurate models, one would consider other methods such as the modified Redfield approach,[78,80,82] hierarchical equations of motion,[28,83−85] iterative linearized density matrix dynamics,[86] non-Markovian quantum state diffusion,[29,87] variational master equation,[88] path integral Monte Carlo,[89] and see the references cited in the review[90] of the methodologies in EET. However, most of these sophisticated methods are not applicable to our large system because they are numerically too demanding.

The effects of slow fluctuations in the site energies (static disorder), which are responsible for the inhomogeneous broadening, are incorporated. We use 100 cm^{-1} for the Gaussian fluctuations in FMO and the baseplate, and 500 cm^{-1} for the roll.[68,70] All results are obtained from 1000 ensemble averages for the static disorder, unless otherwise mentioned.

The system Hamiltonian of FMO trimer complexes is taken from the work of Schmidt am Busch et al.[66] The spectral density from our previous work[30] is used: where molecular dynamics and time-dependent density functional theory calculations were used for obtaining it. A harmonic prefactor was used for the spectral density.[77] The structure of the double wall roll is obtained on the basis of the work of Ganapathy et al.,[56] and the spectral density was obtained by time-dependent density functional theory calculations following the procedure described in Fujita et al.[70]

Instead of computing the spectral density of the baseplate, which is composed of BChl *a*, we use the spectral density of FMO.[30] This approximation is justified because we expect the vibrational structure to be similar to FMO's, which is surrounded by a protein environment (cf., chlorosome) and is also composed of BChl *a*.

To this end, we define the mean exciton energy to quantify the energy dissipation from the system to the bath during the energy funneling process:

$$\mathrm{MEE}(t) = \mathcal{E}(\mathrm{Tr}_S(\hat{H}_S\,\hat{\rho}_S(t))) \tag{1}$$

where $\hat{H}_S$ is the system Hamiltonian and Tr_S is the trace over the system degrees of freedom. $\mathcal{E}$ is the ensemble average over the static disorder.

Additionally, we introduce the exciton cooperativity, which is used to quantify the enhancement of transition dipole moment by coherence. Cooperativity(t), the effective coherent excitation delocalization, is given as follows:

$$\mathrm{Cooperativity}(t) = \frac{1}{|\mu|^2}\mathcal{E}\left(\sum_{\alpha=x,y,z}\ \sum_{m,n\in\mathrm{domain}} \mu_{n,\alpha}\mu_{m,\alpha}\langle n|\hat{\rho}_S(t)|m\rangle\right) \tag{2}$$

where μ_n is the transition dipole moment vector of site n, and a normalization factor $|\mu|^2 = 30\ D^2$, which is the absolute square of the transition dipole moment of a single pigment, is used. The exciton cooperativity reveals the bright state dynamics (i.e., time-dependent emission strength). The complete decoherent mixed state gives the value 1, which implies the exciton "effectively" can be considered to be localized on a single pigment. On the other hand, the coherent dark state gives the value 0, which is not visible in our cooparativity measurement. Accordingly, the cooperativity could give a lower bound to the coherent length. All pigments have the same magnitude of the transition dipole moment in our model (Figure 1B). $|m\rangle$ and $|n\rangle$ are the site basis states. The summation is over the domain of interest.

EXCITATION ENERGY FUNNELING

To fully characterize the exciton transfer process of the photosynthetic apparatus mode in Figure 1, one needs to study the exciton dynamics for all possible initial (exciton) states within an ensemble at a finite temperature. For instance, the initial state prepared by a coherent light source (laser) could be considered as a single exciton state.[91] As an example, we perform exciton dynamics simulations for two cases of initial excitation at 300 K to see how the initial condition affects the EET dynamics. One is the brightest exciton state of the system Hamiltonian of roll A, which is delocalized over roll A (see the snapshot of Figure 3A at 0 ps) and has energy 1018 cm^{-1}. The other initial condition to be considered is a localized initial state (IS). In particular, a single site located on top and in the middle of roll A is selected for the localized IS having energy 3022 cm^{-1} (see the snapshot of Figure 3B at 0 ps).

Comparing the absorption spectra of roll A and roll B in Figure 2A, one can see the peak maximum of roll B is red-shifted from the peak maximum of roll A; thus there is an exciton energy gradient between the layers. As the radius of the roll increases (contrast A and B), the peak maximum shifts to the red.[21,55,92] This occurs because the roll curvature changes, and this induces stronger dipole-dipole interactions between neighboring pigments. This energy gradient is favorable for the exciton energy funneling because EET from the outermost layer to the baseplate is important. Our choice of the initial states on roll A is based on this argument.

There are two important factors in determining the exciton transfer between the antenna units. These are the energy resonance condition and the electronic coupling between the energy levels of the antenna units.[93] The former is the necessary condition for the EET between the units, and the latter determines how fast EET should be. Figure 2 shows the delocalized IS is close to the energy levels of the baseplate and large multichromophoric excitonic coupling strengths to the

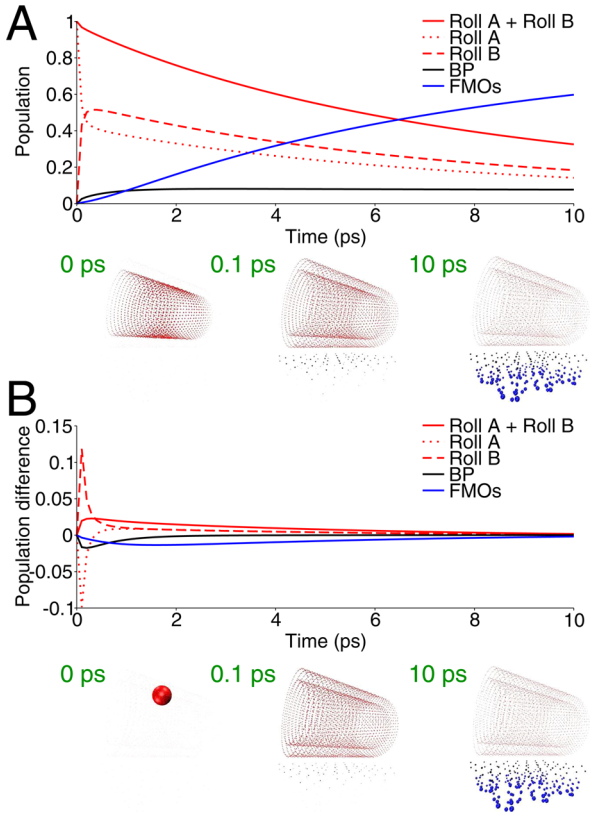

Figure 3. Exciton population dynamics with a delocalized and a localized initial state at 300 K. (A) The initial state (see the snapshot at 0 ps) is the brightest state of roll A. (B) The initial state (see the snapshot at 0 ps) is a localized state, that is, a site on the top and in the middle of roll A. The population difference with respect to the population in (A) is plotted. The locations of magnesium (Mg) in the BChls represent the locations of exciton sites, and the sizes of the spheres are proportional to the populations of the corresponding sites. The populations of the rolls, the baseplate, and the FMOs are designated red, black, and blue, respectively.

baseplate exciton states. In contrast, the localized IS is far from the energy resonance level to the baseplate, and the excitonic coupling strength is small.

Figure 3 summarizes the resulting exciton dynamics at 300 K. Figure 3A and B shows the population dynamics using the delocalized IS and the localized IS, respectively, and up to 10 ps. Our choice of the time interval (10 ps) of the EET simulation is based on the time scales of the EET of *Chlorobium tepidum*.[20] Snapshots of the site populations at 0, 0.1, and 10 ps are shown below the population plots. The exciton population distributions of individual antenna units at 10 ps are almost identical regardless of the initial conditions. For example, the total exciton population on FMOs is approximately 60% for the two initial conditions.

In the rest of this section, we provide a more detailed discussion of severe aspects of the exciton transfer. First, the exciton population dynamics of the two initial conditions are compared. The multichromophoric effect then is discussed for the exciton dynamics. The temperature dependence of the exciton dynamics comes afterward. Last, the exciton dynamics is described in terms of the population kinetic model.

EXCITON POPULATION DYNAMICS

The EET dynamics of the delocalized IS and the localized IS become similar within 1 ps (Figure 3). The short time dynamics (<200 fs), however, are sufficiently different. Figure 3A shows a fast initial population decay for the roll as compared to that of the localized IS in Figure 3B. Characteristic time constants in Table 1 are extracted by the exponential fitting of

Table 1. Time Constants of the Exciton Dynamics of the Chlorosome Roll[a]

set	τ_1 (ps) (A_1 (%))	τ_2 (ps) (A_2 (%))	τ_3 (ps) (A_3 (%))
I[b]	0.081 (3)	4.5 (36)	12.9 (61)
II[c]	0.060 (3)	4.7 (39)	13.1 (58)
III[d]		3.7 (25)	11.3 (75)
ref 20[e]		1.1 (42)	12.1 (58)

[a]The values are obtained by the exponential fittings ($A_1 \exp(-t/\tau_1) + A_2 \exp(-t/\tau_2) + A_3 \exp(-t/\tau_3)$) of the exciton population dynamics for each antenna unit. The amplitudes (A_1, A_2, and A_3) are summed to be 100%. [b]Corresponds to the exciton dynamics of the delocalized IS. [c]Brightest delocalized initial state of roll B is used. The exciton dynamics is given in the Supporting Information. [d]Corresponds to the exciton dynamics of the localized IS. [e]Anisotropic decay of *Chlorobium tepidum* at 807 nm.

the exciton populations of the roll such that amplitudes are summed to be 100%. By comparing the time constants for the roll in Table 1, we see that set I (delocalized IS) has a fast sub-100-fs component, while set III (localized IS) does not. However, τ_1 in set I accounts for only 3% of the 10 ps exciton dynamics. In the case of using the delocalized IS, the single exciton starts to migrate from the roll to the baseplate already at the very beginning (<100 fs). This occurs because the frequency of the delocalized IS (1018 cm^{-1}) is close to the baseplate absorption region (see Figure 2A) and has a large collective transition dipole moment. (Another delocalized IS, which is the brightest exciton state of roll B, shows similar short time dynamics (see set II and the Supporting Information for the corresponding time constants and the exciton dynamics, respectively).) In contrast, the localized IS (3022 cm^{-1}) is far from the energy resonant region and has a comparably weak transition dipole moment.

Equilibration in the roll is achieved within 100 fs for the localized IS dynamics, and almost no exciton population is transferred to the baseplate in this short time. This can be seen in the inset of Figure 4. The inset in Figure 4 shows the diffusion process in the roll with the localized IS for the first 200 fs. Snapshots of the roll populations at 0, 10, and 20 fs are placed above the inset plot. In this plot, one can see how the single exciton diffuses within and between the layers. The black solid line in the inset figure is the mean exciton energy (eq 1), which is normalized to the initial energy (3022 cm^{-1}). Interestingly, the curve is similar to the population dynamics of roll A. From this, we can conclude that the population transfer from roll A to roll B is the main energy relaxation channel, and the slight difference of the two curves indicates the effect of population redistribution within the single layers. Thus, the energy dissipation due to exciton-phonon coupling mainly causes exciton transfer between the layers in this initial short time period. The mean exciton energy of the total system (roll + baseplate + FMOs) is given in Figure 4 for two different initial excitations. The solid blue line and the solid red line

dx.doi.org/10.1021/ja412035q | J. Am. Chem. Soc. 2014, 136, 2048−2057

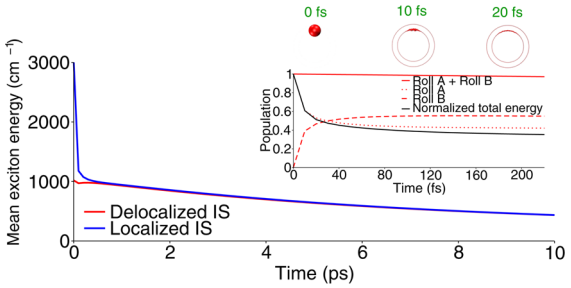

Figure 4. Mean exciton energy with a delocalized and a localized initial state at 300 K. Mean exciton energy (eq 1) with the two different initial excitations, which correspond to those in Figure 3A and B. The short time dynamics for the first 200 fs of Figure 3B is given in the inset with the corresponding population snapshots. The populations in the snapshot are projected to the long axis of the rolls. The locations of magnesium (Mg) atoms in the BChls represent the locations of exciton sites, and the sizes of the spheres are proportional to the populations of the corresponding sites.

correspond to the exciton dynamics of the two different initial conditions, respectively.

As mentioned above, the initial energy of the delocalized state is already close to the baseplate bright state energy domain (see Figure 2), while that of the localized state is higher (3022 cm^{-1}). In the localized IS case, the excess energy (about 2000 cm^{-1}) should be released to the environment for resonant energy transfer to the baseplate to occur. Despite the high initial energy of the localized IS, which is far from the energy resonance domain, the exciton population of each unit at 10 ps is similar to that of the delocalized IS case (see Figure 3A). This is possible because a rapid energy relaxation channel (Figure 2B) is available for the dynamics of set III. The blue line in Figure 4 shows a rapid energy drop within 100 fs. Within 1 ps, the total energy approaches the energy of the delocalized IS. The population snapshots at 100 fs indicate that population distributions are quite similar. Also, the population on the roll in the snapshots of Figure 3B at that time indicates that, by 100 fs, the system population is mostly delocalized over the roll. The mean exciton energies obtained from the exciton dynamics with the delocalized IS and the localized IS become similar within 500 fs. The rapid relaxation within the roll results in robust energy transfer from the roll to the FMOs in the long time limit in our model study.

Microscopically, the energy dissipation dynamics is determined by thermal excitations and relaxation among exciton levels. The energy dissipation rate, in this model, depends on the spectral density, a quantity that indicates how strongly exciton states are coupled to the thermal bath, the probability distribution of the exciton states and temperature.

In Figure 2B, we show the exciton transfer matrix (γ_{MN}) at 300 K in logarithmic scale (log(cm^{-1})). We indicate the fast energy dissipation path for the localized IS with a red arrow. The strong white diagonal band corresponds to the strong exciton-phonon coupling at 1600−2000 cm^{-1} [94] (see the spectral densities in the Supporting Information), which leads to the rapid energy dissipation of the localized IS within the roll. We note here that this fast relaxation occurs only between the exciton states in the same antenna units, and not between the exciton states of different antenna units.

Damjanović et al.[36] suggested that a weakly bound polaron can be formed in BChl aggregates due to the interaction of excitons with intramolecular vibrational mode at about 1670 cm^{-1}. Their results were based on studies of LHC in purple bacteria. We do expect that the polaron couplings can renormalize energy levels and the mobility of the exciton energy is reduced.[36] This should be, however, weaker in the chlorosome where BChls are densely packed and the pigment-pigment interaction is, accordingly, stronger than that of LHC in purple bacteria.

The exciton dynamics in the FMOs is conditioned mainly by the population of the baseplate because direct population transfer from the roll to FMOs is negligible (see the Supporting Information).

COOPERATIVITY OF THE EXCITONIC STATES

In multichromophoric systems, coherent coupling between donor molecules can lead to a large collective transition dipole moment. This enhances the energy transfer from the donor to acceptor groups as compared to incoherent hopping between individual molecules.[12,14,15,95]

In Figure 5, we show the cooperativity (eq 2) computed for first 500 fs. The cooperativity is calculated for the two different

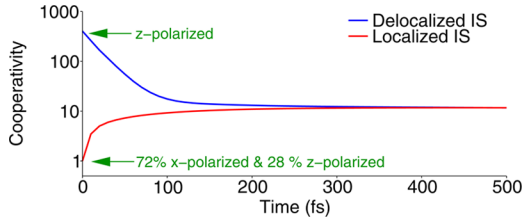

Figure 5. Time-dependent cooperativity of the chlorosome at 300 K. The cooperativity (eq 2), dimensionless normalized collective transition dipole moment, is given in logarithmic scale. During the exciton dynamics in Figure 3 with the two initial states, the cooperativities are calculated for the chlorosome.

initial excitation conditions corresponding to the dynamics in Figure 3.

The delocalized IS is *z*-polarized (along the length of the roll) and initially has a cooperativity of 402 (out of 1620 pigments in roll A). This strong collective oscillator strength can induce rapid supertransfer.[12,14,15] The localized IS, which is 72% *x*- and 28% *z*-polarized, has an initial cooperativity value of unity. This difference in cooperativity at varying initial condition is one of the reasons a fast decay component is found for the delocalized IS case only.

Regardless of the initial conditions, within 500 fs, all cooperativity values converge to a similar value (∼12 out of 3780 pigments in rolls A and B), which is still larger than 1, and the effective transition dipole moment becomes about 30% *x*-, 30% *y*-, and 40% *z*-polarized. This is a favorable situation, for our photosynthetic apparatus model, as *y*-polarization (normal direction to the baseplate) is useful to funnel energy toward the baseplate. These results may indicate a multichromophoric effect;[93] that is, the effective dipole moment of the delocalized exciton state is enhanced by symmetry (see also ref 96 for the discussion on the coherence and EET rate).

TEMPERATURE DEPENDENCE OF THE ENERGY FUNNELING

In the previous subsections, we showed that the exciton energy funneling process is robust to variations in initial excitation conditions due to the fast internal exciton dynamics of the roll. We now investigate the temperature effect by simulating the

dx.doi.org/10.1021/ja412035q | J. Am. Chem. Soc. 2014, 136, 2048−2057

exciton population dynamics with the delocalized IS initial condition, that is, the brightest state of roll A, at 150 and 77 K in Figure 6.

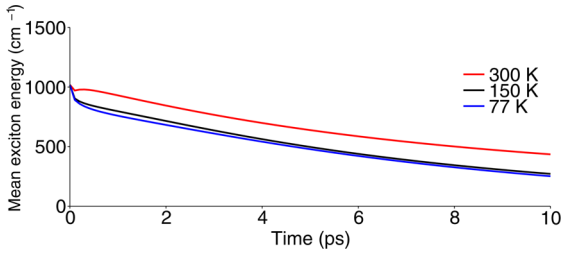

Figure 6. Temperature dependence of the mean exciton energy. The mean exciton energy of the system (eq 1) is plotted at 300, 150, and 77 K. The delocalized exciton initial state in Figure 3A is used.

The mean exciton energy at room temperature (300 K) in Figure 3A is only slightly different from the curves at 150 and 77 K in Figure 6. The corresponding exciton population dynamics are given in the Supporting Information. This indicates that exciton transfer is robust within this temperature range. The robust energy transfer within the temperature range is due to the fast internal exciton dynamics of the roll. The thermal excitation within the temperature range does not lift the exciton far from the energy resonance domain between the roll and the baseplate.

Thermal excitation in the temperature range (77, 150, and 300 K) can provide various channels toward the neighboring exciton states for the relaxation process (see Figure 2B). Thermal excitation can also induce back transfer from the baseplate to the rolls,[95] but it reduces the possibility of being trapped in dark states.

POPULATION KINETICS

So far, we have shown that regardless of initial conditions and temperature, about 60−70% of the exciton can be transferred to the FMOs within 10 ps. This robustness to the choice of initial conditions implies that internal dynamics within the roll is faster than energy transfer between the antenna units. We now proceed to examine the population dynamics by using a simple first-order kinetic model (more sophisticated kinetic models in the EET of the LH complex networks can be found in, e.g., refs 43,44,97,98):

$$\frac{\mathrm{d}}{\mathrm{d}t}\begin{pmatrix}[\mathrm{R}](t)\\ [\mathrm{BP}](t)\\ [\mathrm{FMO}](t)\end{pmatrix} = \begin{pmatrix}-k_{\mathrm{RBP}}(t) & 0 & 0\\ k_{\mathrm{RBP}}(t) & -k_{\mathrm{BPFMO}}(t) & 0\\ 0 & k_{\mathrm{BPFMO}}(t) & 0\end{pmatrix}\begin{pmatrix}[\mathrm{R}](t)\\ [\mathrm{BP}](t)\\ [\mathrm{FMO}](t)\end{pmatrix} \quad (3)$$

where $[\cdot](t)$ denotes the population of each antenna unit, and [R] and [BP] are the populations of the full roll (roll A + roll B) and the baseplate, respectively. $k_{\mathrm{RBP}}(t)$ is the exciton transfer rate from the roll to the baseplate, and $k_{\mathrm{BPFMO}}(t)$ is the one from the baseplate to the FMOs. The population transfer between the antenna units is characterized by time-dependent rate constants $k(t)$. Note that the internal dynamics within the antenna units, such as relaxation and thermal excitation among the exciton states, is incorporated into the time dependence of $k(t)$. $k(t)$ physically corresponds to the multichromophoric Förster resonance energy transfer rate,[93] because it quantifies energy transfer between the donor group (exciton states) of the roll and the acceptor group of the baseplate. The enhancement of energy transfer due to coherence (Figure 5) between donor molecules is also referred as to supertransfer.[12,14,15]

The direct exciton transfer from the roll to the FMO complexes is virtually negligible within the time interval of the EET dynamics 10 ps (see the Supporting Information). In this kinetic model, thus, we assume there is no population transfer from low to high energy units and no direct transfer from the roll to FMOs. The kinetic models are fitted to the exciton populations in Figure 3 using least-squares. The resulting time-dependent population transfer rates are shown in Figure 7 for

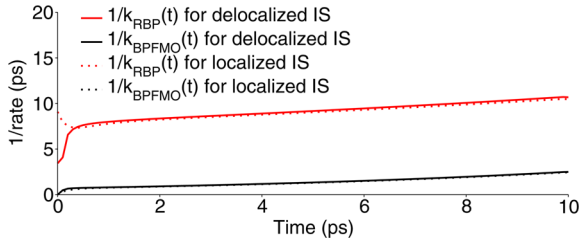

Figure 7. Time-dependent reciprocal rate. Time-dependent exciton transfer rates are given as the corresponding time constants, the reciprocal rate, for the exciton dynamics of the delocalized IS and the localized IS in Figure 3. $k_{\mathrm{RBP}}(t)$: Exciton transfer rate from the roll to the baseplate. $k_{\mathrm{BPFMO}}(t)$: Exciton transfer rate from the baseplate to the FMOs.

the exciton dynamics of Figure 3, using both initial conditions (the delocalized IS and the localized IS). The initial and final values of the reciprocal rates of the (chlorosome) roll $1/k_{\mathrm{RBP}}(t)$ have values similar to τ_2 and τ_3 of sets I and III in Table 1. Within 500 fs, $k_{\mathrm{RBP}}(t)$ for the delocalized IS drops rapidly to a slower rate, with a time scale similar to the equilibrium time of the cooperativity (eq 2); see solid blue line in Figure 5. However, we see that $k_{\mathrm{RBP}}(t)$ for the localized IS does not show this rapid drop. Regardless of the initial conditions, the rate constants become similar to each other within 500 fs. As could be expected, $k_{\mathrm{BPFMO}}(t)$ has no dependence on the initial state in the roll.

CONCLUSION

The green sulfur bacteria are thought to be an incredibly efficient light processing machine (cf., purple bacterium[99]). We studied this system by investigating from an atomistic perspective and a top to bottom approach (cf., Linnanto et al.[100]). The excitation energy transfer route was taken from the chlorosome to the reaction center via the baseplate and FMO, under different initiating conditions. Analysis of the atomistic model indicates that resonant energy transfer is maximized given the multichromophoric excitonic coupling, which is due to the molecular arrangements of these parts: the green sulfur bacteria are assembled to be most conducive toward efficient excitation energy transfer within the Förster energy transfer regime. It was further shown whether the initial excitations are important in the energy funneling process. However, the results differ qualitatively within a short time limit (500 fs). None of these scenarios, however, adversely affect the efficiency of energy transfer, and the results converge within the overall time

dx.doi.org/10.1021/ja412035q | J. Am. Chem. Soc. 2014, 136, 2048−2057

scale (10 ps).[20,23] Thus, the mechanism is robust to initial conditions, including varying temperatures. This is due mainly to the fast internal exciton dynamics of the chlorosome, which is also observed by Fujita et al.[70,75] Furthermore, our measure of cooperativity quantifies this and indicates a preference (again regardless of initial conditions) to the polarization in the *xy*-plane (cross section of the chlorosome), which enhances the excitonic coupling strengths between the exciton states of the chlorosome and the baseplate. We suggest a multichromophoric effect may prevail over the absence of proximity by exploiting the symmetry in parts of the model. This calculation of cooperativity indicates a supertransfer effect inherent in: the green sulfur bacteria, which seems to be especially "tuned" toward thriving under low light conditions by making use of molecular aggregates, symmetry, and self-assembly to capture light and funnel it to the reaction center aided, not hindered, by a fluctuating environment.[26,101]

Additionally, we would like to comment here on the role of the baseplate in the energy funneling process based on our simulations. In our model study, the baseplate plays the role of a "bridge" allowing the exciton energy to funnel down to the FMOs from the chlorosome. The presence of the baseplate eases this process; without the baseplate, energy transfer would be impeded. While it could be the case that transfer is allowed without the baseplate, under the condition that the FMOs and chlorosomes be positioned close enough for Föster energy transfer, our results indicate that the baseplate offers a preferred route. However, the baseplate is considered to be a part of the chlorosome envelope and is likely to be the structure that is involved in its attachment it to the cell membrane.[19] Removal of the baseplate may result in an unstable structure or a different structure altogether. As an alternative working hypothesis for the role of the baseplate, one may consider replacing the BChl *a* molecules in the baseplate with BChl *c* without removing the baseplate structure from the model Hamiltonian. One then may expect no exciton transfer from the chlorosome to FMO complexes because the baseplate is not a J-aggregate, and there is almost no spectral overlap between the baseplate and FMO complexes accordingly.

The baseplate receives the exciton quickly as shown in Figure 3 and releases the exciton to the FMO complexes steadily. Because the chlorosome has a relatively large reorganization energy, which implies strong exciton-phonon couplings to the bath, as compared to those of the baseplate and FMO complexes, the exciton could be lost to the environment if it is able to stay in the chlorosome for too long a time. Thus, we would like to introduce the idea of the baseplate as a biological (single) "exciton capacitor". It seems to be suitably designed for this purpose, making sure the route of the exciton is directed, by receiving the exciton from the chlorosome quickly, keeping the exciton from leaking to the surrounding environment, and supplying it to the FMO. It does so by providing appropriate excitonic sites, via chromophoric pigments, held in a unique and protein scaffold made of amphiphilic units that cross two very different dielectric boundaries (the interim gap between dry lipid chlorosomes and the more watery region at the FMOs) in a near perfect 2D lattice form in analogy to an actual capacitor (condenser) but made of soft materials.

Our model study depends on many undetermined parameters, such as the site energies of the baseplate, distance between the antenna units, and the spectral density of the baseplate. Also, the structure of the chlorosome is still arguable.[52−58] Scanning of these parameters in all combinations is currently not tractable with current computer resources. However, fitting the parameters to experimental data would be useful to determine the structural information of the light-harvesting antenna complexes. Therefore, we postpone this task for future work. Herein, we comment on the two parameters, which would be important to determine the exciton transfer rate between the antenna units. One is the distance between the baseplate and the FMO complexes. We guess the distance would be 1−2 nm, at which range the local pigment to pigment (nearest neighboring pigments between the baseplate and the FMO) transfer rate would be scaled by 10−0.25 in the current model. However, our model study shows the multipigment to multipigment transfer is important, and we expect the overall transfer rate would not be critically changed over this distance range. Exciton delocalization aids in making the transfer less sensitive to the distance change. The second is the site energy of the baseplate. We scanned the site energy of the baseplate with a simplified model system (smaller number of pigments) and found ± 50 cm^{-1} from the current value would result $\pm 20\%$ exciton population difference at 10 ps. Regardless of the uncertainties in the model, our study shows that characteristic time constants fall within sub-100 fs to sub-100 ps and agree with experimental observations[20,23] (see Table 1).

■ ASSOCIATED CONTENT

Supporting Information

Computational details, spectral densities, baseplate lattice model, exciton population dynamics, which are not shown in the Article, and the cumulative density of states of the system. This material is available free of charge via the Internet at http://pubs.acs.org.

■ AUTHOR INFORMATION

Corresponding Authors

huh@fas.harvard.edu

aspuru@chemistry.harvard.edu

Notes

The authors declare no competing financial interest.

■ ACKNOWLEDGMENTS

J.H. thanks Christoph Kreisbeck for the verification of numerical stability in the simulation and discussion about the spectral density. J.H., S.V., T.F., and A.A.-G. acknowledge support from the Center for Excitonics, an Energy Frontier Research Center funded by the U.S. Department of Energy, Office of Science and Office of Basic Energy Sciences under award DE-SC0001088. J.C.B. acknowledges support from Welcome Trust UK. S.K.S. and A.A.-G. also acknowledge Defense Threat Reduction Agency grant HDTRA1-10-1-0046. Further, A.A.-G. is grateful for the support from Defense Advanced Research Projects Agency grant N66001-10-1-4063, and to the Corning Foundation for their generous support.

■ REFERENCES

(1) Blankenship, R. E. *Molecular Mechanisms of Photosynthesis*; World Scientific: London, 2002.

(2) Oostergetel, G. T.; van Amerongen, H.; Boekema, E. J. *Photosynth. Res.* **2010**, *104*, 245−55.

(3) Canfield, D.; Thamdrup, B.; Kristensen, E. *Aquatic Geomicrobiology*; Elsevier: London, 2005.

(4) Overmann, J. In *The Prokaryotes. Vol. 7: Proteobacteria: Delta, Epsilon Subclass*; Dworkin, M., Falkow, S., Rosenberg, E., Schleifer, K.-

H., Stackebrandt, E., Eds.; Springer: New York, 2006; Chapter: The Family Chlorobiaceae, pp 359−378.
(5) Feng, X.; Tang, K.-H.; Blankenship, R. E.; Tang, Y. J. *J. Biol. Chem.* **2010**, *285*, 39544−50.
(6) Overmann, J.; Cypionka, H.; Pfennig, N. *Limnol. Oceanogr.* **1992**, *37*, 150−155.
(7) Beatty, J. T.; Overmann, J.; Lince, M. T.; Manske, A. K.; Lang, A. S.; Blankenship, R. E.; Van Dover, C. L.; Martinson, T. A.; Plumley, F. G. *Proc. Natl. Acad. Sci. U.S.A.* **2005**, *102*, 9306−10.
(8) Manske, A. K.; Glaeser, J.; Kuypers, M. M. M.; Overmann, J. *Appl. Environ. Microbiol.* **2005**, *71*, 8049.
(9) Engel, G.; Calhoun, T.; Read, E.; Ahn, T.; Mancal, T.; Cheng, Y.; Blankenship, R.; Fleming, G. *Nature* **2007**, *446*, 782−786.
(10) Scholes, G. D.; Fleming, G. R.; Olaya-Castro, A.; van Grondelle, R. *Nat. Chem.* **2011**, *3*, 763−74.
(11) Borisov, A. *Biophysics* **2012**, *57*, 562−564.
(12) Lloyd, S.; Mohseni, M. *New J. Phys.* **2010**, *12*, 075020.
(13) Hoyer, S.; Sarovar, M.; Birgitta Whaley, K. *New J. Phys.* **2010**, *12*, 065041.
(14) Abasto, D. F.; Mohseni, M.; Lloyd, S.; Zanardi, P. *Philos. Trans. R. Soc., A* **2013**, *370*, 3750−70.
(15) Kassal, I.; Yuen-Zhou, J.; Rahimi-Keshari, S. *J. Phys. Chem. Lett.* **2013**, *4*, 362−367.
(16) Savikhin, S.; van Noort, P. I.; Zhu, Y.; Lin, S.; Blankenship, R. E.; Struve, W. S. *Chem. Phys.* **1995**, *194*, 245−258.
(17) Psencík, J.; Polvka, T.; Dian, J.; Kudrna, J.; Malý, P. *J. Phys. Chem. A* **1998**, *102*, 4392−4398.
(18) Prokhorenko, V. I.; Steensgaard, D. B.; Holzwarth, A. R. *Biophys. J.* **2000**, *79*, 2105−20.
(19) Psencík, J.; Ma, Y.-Z.; Arellano, J. B.; Hála, J.; Gillbro, T. *Biophys. J.* **2003**, *84*, 1161−79.
(20) Martiskainen, J.; Linnanto, J.; Aumanen, V.; Myllyperkiö, P.; Korppi-Tommola, J. *Photochem. Photobiol.* **2012**, *88*, 675−683.
(21) Fetisova, Z.; Freiberg, A.; Mauring, K.; Novoderezhkin, V.; Taisova, A.; Timpmann, K. *Biophys. J.* **1996**, *71*, 995−1010.
(22) Shibata, Y.; Saga, Y.; Tamiaki, H.; Itoh, S. *Biochemistry* **2007**, *46*, 7062−8.
(23) Martiskainen, J.; Linnanto, J.; Kananavičius, R.; Lehtovuori, V.; Korppi-Tommola, J. *Chem. Phys. Lett.* **2009**, *477*, 216−220.
(24) Mukai, K.; Abe, S.; Sumi, H. *J. Phys. Chem. B* **1999**, *103*, 6096−6102.
(25) Jang, S.; Newton, M. D.; Silbey, R. J. *J. Phys. Chem. B* **2007**, *111*, 6807−14.
(26) Mohseni, M.; Rebentrost, P.; Lloyd, S.; Aspuru-Guzik, A. *J. Chem. Phys.* **2008**, *129*, 174106.
(27) Ishizaki, A.; Fleming, G. R. *Proc. Natl. Acad. Sci. U.S.A.* **2009**, *106*, 17255−60.
(28) Strümpfer, J.; Schulten, K. *J. Chem. Phys.* **2009**, *131*, 225101.
(29) Ritschel, G.; Roden, J.; Strunz, W. T.; Aspuru-Guzik, A.; Eisfeld, A. *J. Phys. Chem. Lett.* **2011**, *2*, 2912−2917.
(30) Shim, S.; Rebentrost, P.; Valleau, S.; Aspuru-Guzik, A. *Biophys. J.* **2012**, *102*, 649−60.
(31) Kreisbeck, C.; Kramer, T. *J. Phys. Chem. Lett.* **2012**, *3*, 2828−2833.
(32) Kim, H. W.; Kelly, A.; Park, J. W.; Rhee, Y. M. *J. Am. Chem. Soc.* **2012**, *134*, 11640−51.
(33) Celardo, G. L.; Borgonovi, F.; Merkli, M.; Tsifrinovich, V. I.; Berman, G. P. *J. Phys. Chem. C* **2012**, *116*, 22105−22111.
(34) Christensson, N.; Kauffmann, H. F.; Pullerits, T.; Mančal, T. *J. Phys. Chem. B* **2012**, *116*, 7449−54.
(35) Chenu, A.; Christensson, N.; Kauffmann, H. F.; Mančal, T. *Sci. Rep.* **2013**, *3*, 2029.
(36) Damjanovič, A.; Kosztin, I.; Kleinekathöfer, U.; Schulten, K. *Phys. Rev. E* **2002**, *65*, 1−24.
(37) Olbrich, C.; Kleinekathöfer, U. *J. Phys. Chem. B* **2010**, *114*, 12427−37.
(38) Hu, X.; Ritz, T.; Damjanovic, A.; Schulten, K. *J. Phys. Chem. B* **1997**, *101*, 3854−3871.
(39) Sener, M. K.; Olsen, J. D.; Hunter, C. N.; Schulten, K. *Proc. Natl. Acad. Sci. U.S.A.* **2007**, *104*, 15723−8.
(40) Olaya-Castro, A.; Lee, C.; Olsen, F.; Johnson, N. *Phys. Rev. B* **2008**, *78*, 085115.
(41) Ringsmuth, A. K.; Milburn, G. J.; Stace, T. M. *Nat. Phys.* **2012**, *8*, 562−567.
(42) Dostál, J.; Mančal, T.; Augulis, R.; Vácha, F.; Pšenčk, J.; Zigmantas, D. *J. Am. Chem. Soc.* **2012**, *134*, 11611−7.
(43) Cao, J.; Silbey, R. J. *J. Phys. Chem. A* **2009**, *113*, 13825−38.
(44) Caruso, F.; Chin, A. W.; Datta, A.; Huelga, S. F.; Plenio, M. B. *J. Chem. Phys.* **2009**, *131*, 105106.
(45) Bennett, D. I. G.; Amarnath, K.; Fleming, G. R. *J. Am. Chem. Soc.* **2013**, *135*, 9164−9173.
(46) Pedersen, M. O.; Linnanto, J.; Frigaard, N.-U.; Nielsen, N. C.; Miller, M. *Photosynth. Res.* **2010**, *104*, 233−43.
(47) Olson, J. M. *Photosynth. Res.* **2004**, *80*, 181−187.
(48) Föster, T. *Ann. Phys.* **1948**, *437*, 55−75.
(49) May, V.; Kühn, O. *Charge and Energy Transfer Dynamics in Molecular Systems*, 3rd ed.; Wiley-VCH: New York, 2011.
(50) Zimanyi, E. N.; Silbey, R. J. *Philos. Trans. R. Soc., A* **2012**, *370*, 3620−37.
(51) Frigaard, N.-U.; Chew, A. G. M.; Li, H.; Maresca, J. A.; Bryant, D. A. *Photosynth. Res.* **2003**, *78*, 93−117.
(52) Holzwarth, A. R.; Schaffner, K. *Photosynth. Res.* **1994**, *41*, 225−233.
(53) Frese, R.; Oberheide, U.; Stokkum, I. V.; Grondelle, R. V.; Foidl, M.; Amerongen, H. V. *Photosynth. Res.* **1997**, *54*, 115−126.
(54) Psencík, J.; Ikonen, T. P.; Laurinmäki, P.; Merckel, M. C.; Butcher, S. J.; Serimaa, R. E.; Tuma, R. *Biophys. J.* **2004**, *87*, 1165−1172.
(55) Linnanto, J. M.; Korppi-Tommola, J. E. I. *Photosynth. Res.* **2008**, *96*, 227−45.
(56) Ganapathy, S.; Oostergetel, G. T.; Wawrzyniak, P. K.; Reus, M.; Gomez Maqueo Chew, A.; Buda, F.; Boekema, E. J.; Bryant, D. A.; Holzwarth, A. R.; de Groot, H. J. M. *Proc. Natl. Acad. Sci. U.S.A.* **2009**, *106*, 8525−30.
(57) Ganapathy, S.; Oostergetel, G. T.; Reus, M.; Tsukatani, Y.; Gomez Maqueo Chew, A.; Buda, F.; Bryant, D. A.; Holzwarth, A. R.; de Groot, H. J. *Biochemistry* **2012**, *51*, 4488−98.
(58) Tang, J. K.-H.; Saikin, S. K.; Pingali, S. V.; Enriquez, M. M.; Huh, J.; Frank, H. A.; Urban, V. S.; Aspuru-Guzik, A. *Biophys. J.* **2013**, *105*, 1346−1356.
(59) Tian, Y.; Camacho, R.; Thomsson, D.; Reus, M.; Holzwarth, A. R.; Scheblykin, I. G. *J. Am. Chem. Soc.* **2011**, *133*, 17192−9.
(60) Pedersen, M. O. S.; Underhaug, J.; Dittmer, J.; Miller, M.; Nielsen, N. C. *FEBS Lett.* **2008**, *582*, 2869−74.
(61) Phillips, J.; Braun, R.; Wang, W.; Gumbart, J.; Tajkhorshid, E.; Villa, E.; Chipot, C.; Skeel, R.; Kale, L.; Schulten, K. *J. Comput. Chem.* **2005**, *26*, 1781−1802.
(62) Hornak, V.; Abel, R.; Okur, A.; Strockbine, B.; Roitberg, A.; Simmerling, C. *Proteins* **2006**, *65*, 712−25.
(63) Blankenship, R. E.; Madigan, M. T.; Bauer, C. E. *Anoxygenic Photosynthetic Bacteria*; Kluwer Academic Publishers: New York, 1995.
(64) Tronrud, D. E.; Wen, J.; Gay, L.; Blankenship, R. E. *Photosynth. Res.* **2009**, *100*, 79−87.
(65) Wen, J.; Zhang, H.; Gross, M. L.; Blankenship, R. E. *Proc. Natl. Acad. Sci. U.S.A.* **2009**, *106*, 6134−9.
(66) Schmidt am Busch, M.; Müh, F.; El-Amine Madjet, M.; Renger, T. *J. Phys. Chem. Lett.* **2011**, *2*, 93−98.
(67) Adolphs, J.; Renger, T. *Biophys. J.* **2006**, *91*, 2778−97.
(68) Milder, M. T. W.; Brüggemann, B.; van Grondelle, R.; Herek, J. L. *Photosynth. Res.* **2010**, *104*, 257−74.
(69) Francke, C.; Amesz, J. *Photosynth. Res.* **1997**, 137−146.
(70) Fujita, T.; Brookes, J. C.; Saikin, S. K.; Aspuru-Guzik, A. *J Phys. Chem. Lett.* **2012**, *3*, 2357−2361.
(71) Louisell, W. H. *Quantum Statistical Properties of Radiation*; John Wiley & Sons: New York, 1973.
(72) Breuer, H. P.; Petruccione, F. *The Theory of Open Quantum Systems*; Oxford University: Oxford, 2006.

(73) Rebentrost, P.; Chakraborty, R.; Aspuru-Guzik, A. *J. Chem. Phys.* **2009**, *131*, 184102.
(74) Rebentrost, P.; Mohseni, M.; Aspuru-Guzik, A. *J. Phys. Chem. B* **2009**, *113*, 9942−7.
(75) Fujita, T.; Huh, J.; Saikin, S. K.; Brookes, J. C.; Aspuru-Guzik, A. arXiv:1304.4902v2, 2013.
(76) Ishizaki, A.; Fleming, G. R. *J. Chem. Phys.* **2009**, *130*, 234110.
(77) Valleau, S.; Eisfeld, A.; Aspuru-Guzik, A. *J. Chem. Phys.* **2012**, *137*, 224103.
(78) Zhang, W. M.; Meier, T.; Chernyak, V.; Mukamel, S. *J. Chem. Phys.* **1998**, *108*, 7763.
(79) Pullerits, T. *J. Chin. Chem. Soc.* **2000**, *47*, 773−784.
(80) Yang, M.; Fleming, G. R. *Chem. Phys.* **2002**, *275*, 355−372.
(81) Novoderezhkin, V.; Salverda, J. M.; Amerongen, H. V. *J. Phys. Chem. B* **2003**, *107*, 1893−1912.
(82) Novoderezhkin, V. I.; Palacios, M. A.; Amerongen, H. V. *J. Phys. Chem. B* **2004**, *108*, 10363−10375.
(83) Ishizaki, A.; Fleming, G. R. *J. Chem. Phys.* **2009**, *130*, 234111.
(84) Kreisbeck, C.; Kramer, T.; Rodrguez, M.; Hein, B. *J. Chem. Theory Comput.* **2011**, *7*, 2166−2174.
(85) Zhu, J.; Kais, S.; Rebentrost, P.; Aspuru-Guzik, A. *J. Phys. Chem. B* **2011**, *115*, 1531−7.
(86) Huo, P.; Coker, D. F. *J. Phys. Chem. Lett.* **2011**, *2*, 825−833.
(87) Ritschel, G.; Roden, J.; Strunz, W. T.; Eisfeld, A. *New J. Phys.* **2011**, *13*, 113034.
(88) Mccutcheon, D. P. S.; Nazir, A. *J. Chem. Phys.* **2011**, *135*, 114501.
(89) Mühlbacher, L.; Kleinekathöfer, U. *J. Phys. Chem. B* **2012**, *116*, 3900−6.
(90) Pachón, L. A.; Brumer, P. *Phys. Chem. Chem. Phys.* **2012**, *14*, 10094−108.
(91) Brumer, P.; Shapiro, M. *Proc. Natl. Acad. Sci. U.S.A.* **2012**, *109*, 19575−8.
(92) Prokhorenko, V. I.; Steensgaard, D. B.; Holzwarth, A. R. *Biophys. J.* **2003**, *85*, 3173−86.
(93) Jang, S.; Newton, M.; Silbey, R. *Phys. Rev. Lett.* **2004**, *92*, 218301−4.
(94) Roden, J.; Schulz, G.; Eisfeld, A.; Briggs, J. *J. Chem. Phys.* **2009**, *131*, 044909.
(95) Causgrove, T. P.; Brune, D. C.; Blankenship, R. E. *J. Photochem. Photobiol., B: Biol.* **1992**, *15*, 171−9.
(96) Strümpfer, J.; Sener, M.; Schulten, K. *J. Phys. Chem. Lett.* **2012**, *3*, 536−542.
(97) Yang, M.; Fleming, G. R. *J. Chem. Phys.* **2003**, *119*, 5614.
(98) Valkunas, L.; Chmeliov, J.; Trinkunas, G.; Duffy, C. D. P.; van Grondelle, R.; Ruban, A. V. *J. Phys. Chem. B* **2011**, *115*, 9252−60.
(99) Hildner, R.; Brinks, D.; Nieder, J. B.; Cogdell, R. J.; van Hulst, N. F. *Science* **2013**, *340*, 1448−1451.
(100) Linnanto, J. M.; Korppi-tommola, J. E. I. *J. Phys. Chem. B* **2013**, *117*, 11144−11161.
(101) Rebentrost, P.; Mohseni, M.; Kassal, I.; Lloyd, S.; Aspuru-Guzik, A. *New J. Phys.* **2009**, *11*, 033003.